Non-Periodic Gait Planning Based on Salient Region Detection for a Planetary Cave Exploration Robot

NON-PERIODIC GAIT PLANNING BASED ON SALIENT REGION DETECTION FOR A PLANETARY CAVE EXPLORATION ROBOT

Virtual Conference 19-23 October 2020

Kentaro Uno[1], Yusuke Koizumi[1], Keigo Haji[1], Maximilian Keiff[2], Simon Harms[3], Warley F. R. Ribeiro[1], William Jones[1], Kenji Nagaoka[4], Kazuya Yoshida[1]

[1]Department of Aerospace Engineering, Tohoku University, Aoba 6-6-01, Aramaki, Aoba-ku, Sendai, Miyagi 980-8579, Japan, Email: {unoken, yusuke.koizumi.s3, keigo.haji.q3, warley, william}@dc.tohoku.ac.jp, yoshida@astro.mech.tohoku.ac.jp

[2]Paderborn University, Germany, E-mail: mkeiff@campus.uni-paderborn.de

[3]Institute of Space Systems, Technical University of Braunschweig, Hermann-Blenk-Str. 23, 38108 Braunschweig, Germany, E-mail: simon.harms@tu-braunschweig.de

[4]Department of Mechanical and Control Engineering, Kyushu Institute of Technology, Sensuicho 1-1, Tobata-ku, Kitakyushu, Fukuoka 804-8550, Japan, E-mail: nagaoka.kenji572@mail.kyutech.jp

ABSTRACT

A limbed climbing robot can traverse uneven and steep terrain, such as Lunar/Martian caves. Towards the autonomous operation of the robot, we first present a method to detect topographically salient regions in 3D point cloud as the robot ' s graspable targets, and next, we introduce a strategy to plan a non-periodic gait for the robot from the detected discrete graspable options. The proposed gait planner is implemented and validated in our open dynamic climbing robot simulation platform assuming the 3 kg class four-limbed climbing robot testbed moving over steep and uneven Lunar terrain.

1 INTRODUCTION

A limbed climbing robot demonstrates exceptional capabilities of traversing uneven and steep terrain. Thus, they can be identified as a key technology to enable and increase the coverage by robotic exploration on planetary surfaces [1], such as overcoming bedrocks, cliffs, and even the inside of planetary caves. Particularly, potential Lunar lava tubes [2, 3] and Martian caves [4] are kind of places that are expected to yield great scientific potential. These locations also represent potential places for mid to long-term habitation on the Moon since they offer natural protection from cosmic radiation, direct sunlight, and a thermal gap for the temperature differential between daytime and nighttime [5, 6]. For the initial exploration missions, climbing mobile robotic platforms will play a vital role.

For climbing locomotion in rocky terrain, a spine-type gripper shows great effectiveness as demonstrated by NASA/JPL LEMUR3 microspine gripper [7] and Tohoku Univ./Space Robotics Lab. (SRL) passive spine gripper [8]. To optimize a spine-type gripper's performance to secure climbing locomotion, it is essential to extract graspable topographies; these graspable topographies may then provide discrete options for locomotion/gripper control algorithms.

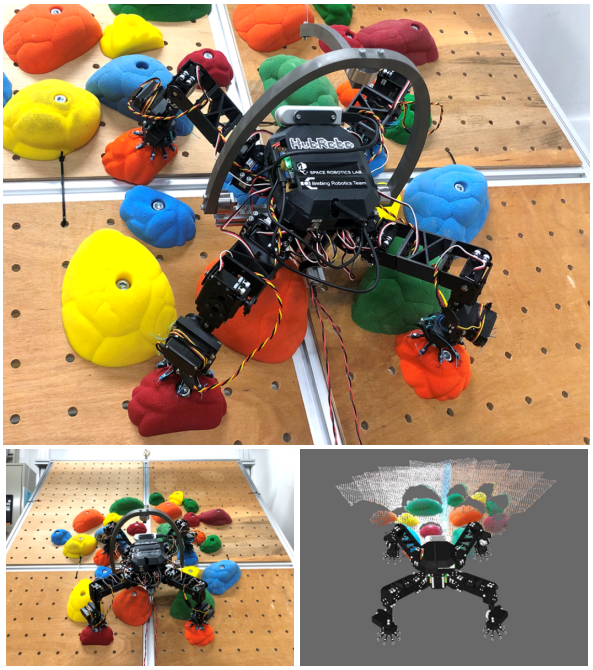

Figure 1: HubRobo on steep inclined uneven terrain. The climbing robot should sense the shape of terrain and select the proper gripping target for the autonomous exploration.

In this paper, first we present an algorithm that can extract convex structures from a point cloud of terrain data. The algorithm is performed based on the size and shape of the grasping workspace of the gripper; it can

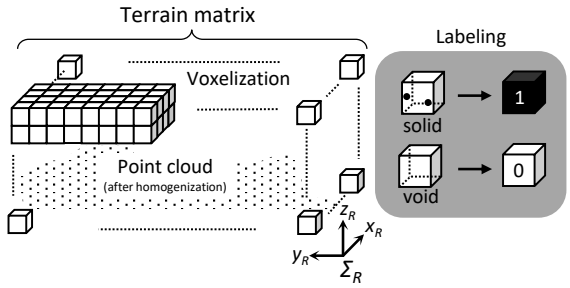

Figure 2 : Conceptual illustlation how to produce a terrain matrix.

further customize results by adjusting the gripper's geometric parameters e.g. diameter of the gripper palm. Based on the graspable salient output distribution, we then implement a non-periodic limb selection and a gripping point selection in the gait planning algorithm reported in [9]. This non-periodic gait is assessed in dynamic simulations performed by an open-sourced dynamic climbing robot simulator: ClimbLab[1], assuming that our four-limed climbing robot testbed: HubRobo (mass: 3.0 kg with battery, degree of freedom: three per limb, shown in Fig. 1) climbs up the steep slope on the Lunar surface.

2 SALIENT REGION DETECTION

In robotics, salient region/object detection is commonly used for object recognition in robot hand manipulation. In related works, RGB image based salient object extraction techniques are reported and the recent success of machine learning helps to increase the accuracy [10, 11].

For our application, the color data cannot be utilized to its maximum potential because there is little observable color contrast in natural rocky terrains. As a related work about topographically salient region detection using point cloud, [12] reported the way to extract salient features in a 3D mesh. In our case, in addition to the feature saliency, graspable targets are also required to have an appropriate size and sharpness to fit in the graspable space of the gripper. Particularly for the spine type gripper that is installed in HubRobo in [8], a convex shape is preferred rather than a flat or concave shape. Eventually, the problem is defined as finding the proper shapes from a point cloud. Hereafter, we present a technique to extract this information from sensor data acquired by the robot.

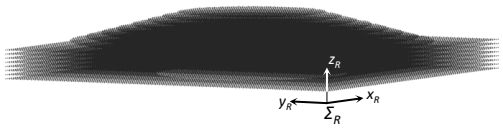

Figure 3 : Appearance of the gripper mask designed for the passive spine gripper [8]. Black dots represent solid cells.

2.1 Terrain Matrix

To perform the computation efficiently, a raw point cloud is represented as a terrain matrix, which is the input to the algorithm of our function. Terrain matrix representation is performed to the raw point cloud in the following steps:

1. Coordinate transformation: the coordinates are transformed to the fixed on referential of the regression plane obtained from raw point cloud: Σ_R in such a way where z axis is aligned with the normal direction of the regression plane.

2. Occlusion compensation: the occluded area is linearly interpolated by Delaunay triangulation. As a result of this operation, the density of point cloud is homogenized.

3. Voxelization and labeling: the homogeneously distributed point cloud space is voxelized where each voxel is labeled as either solid: 1 or void: 0 depending on the voxel has point clouds or not.

Through this operation, a three-dimensional matrix which consists of elements equal to either 1 or 0, and is defined as terrain matrix: M_t.

2.2 Gripper Mask

Gripper mask: M_g is a three-dimensional matrix with the same pitch as the terrain matrix. M_g's solid (=1) elements represent the ideal shape for the assumed gripper.

In the case of an asymmetrical gripper, the mask is designed as a circular truncated conic shape based on the angular movable range of the fingers, and the pitch, i.e. the distance between every two elements is set as 1 mm. The final aspect of the gripper mask used for this study is shown in Fig. 3.

2.3 Salient Region Detection

The algorithm presented here, in essence, consists of scanning the terrain matrix with the gripper mask to find

[1] Available at https://github.com/Space-Robotics-Laboratory/ClimbLab

correspondences. The algorithm picks a solid voxel, assuming its index is i, in the terrain matrix and then, extracts a partial matrix: M_t^i that has the same size as the gripper mask around voxel i. Here, this extraction is only performed on the solid voxels in the terrain matrix, which helps to reduce unnecessary computation. Next, picking a solid cell: $m_{t,jkl}^i (= 1)$ in M_t^i (here, assume the solid cell is (j,k,l) element), it assesses whether there exists same elements in $M_g : m_{g,jkl}$ that also holds the value of 1. If this condition is satisfied for all solid elements in M_t^i, the selected voxel i is set as the center of the shape that is sufficiently similar to the gripper mask, i.e., graspable.

We applied this technique on uneven terrain: a group of climbing holds. Fig. 4 presents the process to obtain the graspable results within the field of view of the robot. Fig. 4(a) shows the target objects and (b) is the raw point cloud of the target, where we used intel RealSense D435 to acquire the point cloud. (c) shows generated the terrain matrix from (b), where we set the voxel size: 1 mm. Applying the proposed technique with the terrain matrix, we can obtain the positions of graspable salient regions within the terrain as shown in (d).

(a) Appearance of the gripper mask.

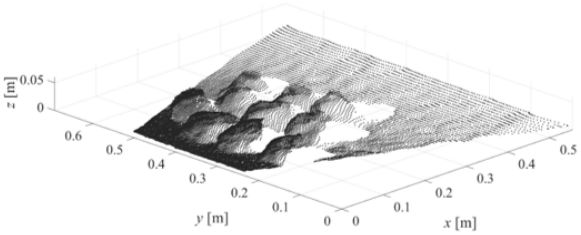

(b) Raw point cloud.

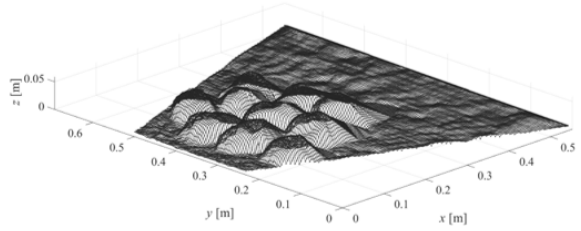

(c) Visualization of terrain matrix drawn as mesh.

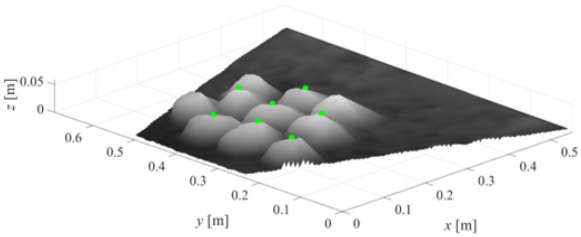

(d) Result output of the algorithm.

Figure 4 : Process of graspable target detection. Green dots in (d) represent the graspable points.

3 ADAPTATION OF GAIT PLANNER

In our previous work, we proposed a gait planner for a four-legged climbing robot, where the robot selects the next grasping point to obtain the longest stride that is kinematically feasible while approaching the goal with a periodic limb locomotion [9]. To adapt the gait in [9] to the graspable salient output distribution, a non-periodic selection of the limb to be transferred to next gripping point (hereafter, we call this free leg swing limb) is implemented. In the updated gait planner, the limb that has the most graspable options in the direction of the target location is selected. The following sections elaborate on the updated gait planner.

3.1 Swing Limb Selection

A periodic fixed sequence of swing limbs leads potential inefficiencies in terms of time and energy consumption in case the graspable points are discrete at random. Therefore, in the presented gait planner, non-periodicity is implemented in the selection of the swing limb. Specifically, first for every limb, in its reachable region, the number of graspable options in the side of moving direction, is counted. Then, the limb which has the most graspable targets is selected to be swung next. In the case of Fig. 5, the number is 1 for left front (LF) limb, 2 for left hind (LH) limb, 3 for right hind (RH) limb, and 2 right front (RF) limb, therefore the swing limb is RH limb. This strategy is based on the following simple assumptions: 1) a limb with more graspable options tends to have a high potential for a bigger stride, and 2) a limb with more graspable options tends to be the most delayed limb behind the base movement, and thereby the presented swing limb selection contributes to increase the efficiency in the whole robot motion.

3.2 Gripping Point Selection

After the optimal selection of the swing limb, the actual gripping point then needs to be decided. In this work, we use the same technique presented in [9]; the next gripping point is selected so that the robot can get the longest stride to move forward within the kinematic

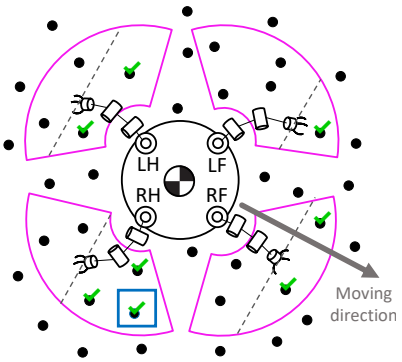

Figure 5 : How to select the next swing limb and gripping point. In this case, the right hind (RH) limb gets selected to grip the point (marked with blue square) to gain the longest step to move along with the direction to the goal.

constraint.

3.3 Limb and Base Motion Planning

A limb motion trajectory is generated as a third-order spline polynomial with a given swing height the same as our previous work in [13]. Simultaneously, the base motion is executed at each swing phase in the way that the projection of the robot center of mass (CoM) is to be put on the intersection of the diagonal lines of limbs [9]. Though this CoM projection-based motion planning can only be applied for climbing on a slope, in this paper, the same strategy is applied to evaluate the non-periodicity in the gait comparing the results with our previous periodic gait planner. In another article, we have proposed a method of evaluating the stability of the robot climbing on a vertical wall and ceiling [14].

4 CLIMBING SIMULATION

To validate the proposed gait planner, we performed dynamic simulations assuming HubRobo is climbing up a steep slope (inclination angle: 30 deg) under Lunar gravity. For the simulation platform, we use ClimbLab - climbing robot MATLAB simulator, which is recently open-sourced by our research group.

4.1 Simulation Conditions

Detailed simulation conditions are as follows:

- Robot: HubRobo version 3.1 (Fig. 1)
- Maximum gripping force: 9.0 N
- Swing height: 0.02 m
- Base height from the ground: 0.06 m
- Time period of swing limb: 4 s
- Demonstrated gravity: $G/6$ (Lunar gravity)

In this simulation, HubRobo version 3.1 without batteries (mass: 2.3 kg) is assumed, and quasistatic gait is executed, where there is no phase of four limbs supporting. As for the maximum gripping force, which is the maximum endurable value of an external pulling force to the gripper (hereafter it is called simply holding force), our pulling experiments showed an average holding force of 6.8 N. Since the latest version of HubRobo has 8 fingers for the gripper while 6 fingers in the previous model, we multiply 8/6 to 6.8 N as the holding force.

An infinite discrete graspable point map is prepared for the simulation. The map is created by connecting multiple copies of the results from the salient detection against a group of climbing holds.

4.2 Simulation Results

Fig. 6 shows the overall result of the two simulations: one is performed using the previous periodic gait planner in [9] and the other with the proposed non-periodic gait planner. Fig. 7 shows the time histories of the robot base position in the moving direction: x in Σ_R. From the simulation, Tumble Stability Margin (TSM) [15], a quantitative method to evaluate the stability of the walking and climbing robot, is also measured (Fig. 8). Although there are few moments when TSM equals to zero in the case of the non-periodic gait, any tumbling phenomena are observed in the simulation. As a whole, any significant difference of TSM is observed between the two simulations.

4.3 Discussions

As demonstrated in Fig. 6, both gait planners worked successfully to operate the robot to climb up the slope without tumbling. In Fig. 7, the non-periodic gait planner enabled the robot to move 0.17 m in 45 s. In contrast, spending the same time period, the robot with the previous periodic gait planner just completed approximately 0.8 m. This can be explained by which the periodic gait control selects the swing limb in a predetermined sequence. Thus, the periodic gait often executes less optimal steps in terms of the stride length. Moreover, from Fig. 7 and Fig. 8, the non-periodic swing limb selection can improve time and energy efficiency, sustaining safe TSM.

5 CONCLUSION

In this study, we presented a strategy to plan an optimal gait on the detected graspable options towards an autonomous locomotion of a climbing robot that plays an important role in exploration missions in planetary

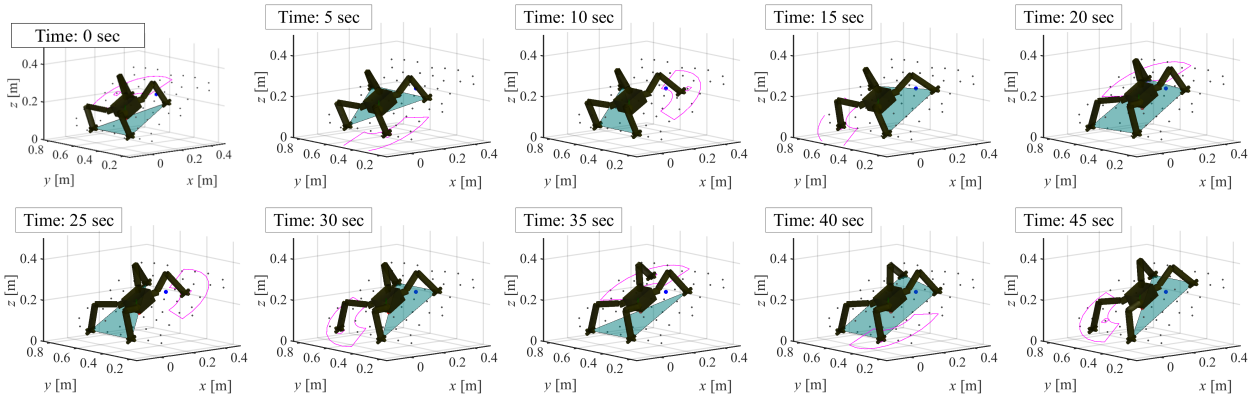

(a) Previous periodic gait [9]

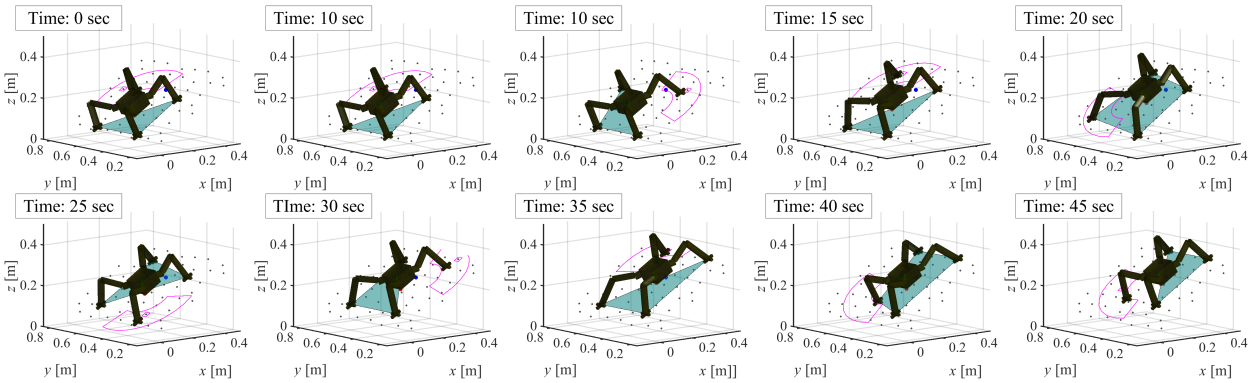

(b) Proposed non-periodic gait

Figure 6 : Time history of the robot climbing simulation where random discrete graspable points are given on a 30° inclined slope under Lunar gravity. In the simulation animations, the CoM projection point (red circle), goal point (blue circle), support polygon (light blue), and reachable region of swing limb (pink) are illustrated, respectively.

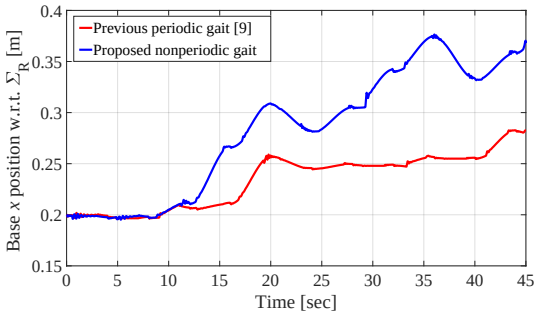

Figure 7 : Time histories of robot base postion in the two simulations. New non-periodic gait planner operates the robot move twice faster than the previous gait planner.

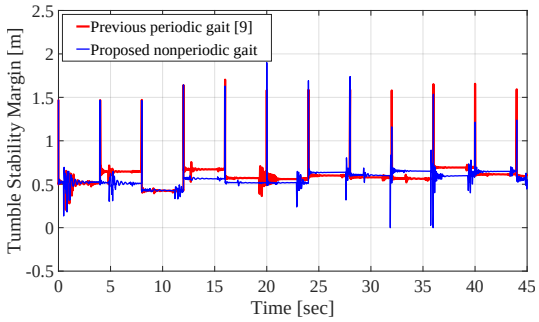

Figure 8 : Time histories of Tumble Stability Margin (TSM) while the two simulations.

caves. First, we proposed a technique to detect topographically convex structures from raw point cloud terrain data. We then updated the previous gait planner by implementing a non-periodic swing limb selection.

Moreover, as an initial assessment of the proposed non-periodic gait, we performed dynamic robot simulations climbing on steep terrain under lunar gravity, using a model of our robot testbed HubRobo. Comparing the simulation results using the two gait planners, the pre-

viously developed periodic gait, and the proposed non-periodic gait in this work, it was found that the adaptive non-periodicity in swing limb selection contributes to reducing the time and energy consumption required to reach the goal state by about 50 percent on average.

Future work incorporating the proposed non-periodic gait planner will update base motion planning in accordance with the Stability Polyhedron [14]. Also, to validate the climbing performance in the real world, climbing experiments using the real HubRobo hardware will be conducted. Finally, using a deep reinforcement learning (RL) based motion planner that is currently in development in ClimbLab, we will compare the model-free RL approach [16] with the model-based approach outlined in this paper.

Acknowledgement

This work is supported by JSPS KAKENHI Grant Number 19J20685.

References

[1] Yoshida K, Maruki T, and Yano H (2002) A novel strategy for asteroid exploration with a surface robot. In: *Proceedings of the 34th COSPAR Scientific Assembly*, pp. 281–286.

[2] Haruyama J, Hioki K, Shirao M, Morota T, Hiesinger H, van der Bogert CH, Miyamoto H, Iwasaki A, Yokota Y, Ohtake M, Matsunaga T, Hara S, Nakanotani S, and Pieters CM (2009) Possible lunar lava tube skylight observed by SELENE cameras. *Geophysical Research Letters*, 36(21): Art. no. L21206, doi: 10.1029/2009GL040635.

[3] Kaku T, Haruyama J, Miyake W, Kumamoto A, Ishiyama K, Nishibori T, Yamamoto K, Crites ST, Michikami T, Yokota Y, Sood R, Melosh HJ, Chap-paz L, and Howell KC (2017) Detection of intact lava tubes at Marius hills on the moon by SELENE (Kaguya) lunar radar sounder. *Geophysical Research Letters*, 44(20): pp. 10,155–10,161. doi: 10.1002/2017GL074998.

[4] Cushing GE, Titus TN, Wynne JJ, and Christensen PR (2007) THEMIS observes possible cave skylights on mars. *Geophysical Research Letters* 34(17): Art. no. L17201. doi: 10.1029/2007GL030709.

[5] Hörz, F (1985) In: *Lunar bases and space activities of the 21st century.*, Mendell WW ed. Lunar and Planetary Institute, Houston, pp. 405–412.

[6] Haruyama J, Morota T, Kobayashi S, Sawai S, Lucey PG, Shirao M, and Hishino MN (2012) *Lunar holes and lava tubes as resources for lunar science and exploration.*, In: *Moon.* Springer, Berlin, Heidelberg. pp. 139–163. doi: 10.1007/978-3-642-27969-0_6.

[7] Parness A, Abcouwer N, Fuller C, Wiltsie N, Nash J, and Kennedy B (2017) LEMUR 3: A limbed climbing robot for extreme terrain mobility in space. In: *Proceedings of the 2017 IEEE International Conference on Robotics and Automation (ICRA)*, Marina Bay Sands, Singapore, pp. 5467–5473. doi: 10.1109/ICRA.2017.7989643.

[8] Nagaoka K, Minote H, Maruya K, Shirai Y, Yoshida K, Hakamada T, Sawada H, and Kubota T (2018) Passive spine gripper for free-climbing robot in extreme terrain. *IEEE Robotics and Automation Letters.*, 3(3): pp. 1765–1770. doi: 10.1109/LRA.2018.2794517.

[9] Uno K, Ribeiro WFR, Jones W, Shirai Y, Minote H, Nagaoka K, and Yoshida K (2019) Gait planning for a free-climbing robot based on tumble stability. In: *Proceedings of the 2019 IEEE/SICE International Symposium on System Integration (SII)*, Paris, France, pp. 289–294. doi: 10.1109/SII.2019.8700455.

[10] Wang W, Zhao S, Shen J, Hoi SCH, and Borji A (2019) Salient object detection with pyramid attention and salient edges. In: *Proceedings of the IEEE/CVF Conference on Computer Vision and Pattern Recognition (CVPR)*, Marina Bay Sands, Singapore, pp. 1448–1457. doi: 10.1109/CVPR.2019.00154.

[11] Wang W, Lai Q, Fu H, Shen J, Ling H, and Yang R (2019) Salient object detection in the deep learning era: an in-depth survey. arXiv:1904.09146.

[12] Hisada M, Belyaev AG, Kunii TL (2002) A skeleton-based approach for detection of perceptually salient features on polygonal surfaces. *Computer Graphics Forum.*, 21(4): pp. 689–700. doi: 10.1111/1467-8659.00627.

[13] Ribeiro WFR, Uno K, Nagaoka K, Yoshida K (2019) Analysis of motion control for a quadruped ground-gripping robot for minor body exploration. In: *Proceedings of the 32nd International Symposium on Space Technology and Science*, Fukui, Japan, #2019-k-33, 2019.

[14] Ribeiro WFR, Uno K, Nagaoka K, Yoshida K (2020) Dynamic equilibrium of climbing robots based on stability polyhedron for gravito-inertial acceleration. In: *Proceedings of the CLAWAR 2020: 23rd International Conference on Climbing and Walking Robots and the Support Technologies for Mobile Machines*, Moscow, Russian Federation, pp. 297–304. doi: 10.13180/clawar.2020.24-26.08.18.

[15] Yoneda K, Hirose S (1996) Tumble stability criterion of integrated locomotion and manipulation. In: *Proceedings of the IEEE/RSJ International Conference on Intelligent Robots and Systems (IROS)*, Osaka, Japan, pp. 870–876. doi: 10.1109/IROS.1996.571067.

[16] Jones W, Blum T, Yoshida K (2020) Adaptive slope locomotion with deep reinforcement learning. In: *Proceedings of the 2019 IEEE/SICE International Symposium on System Integration (SII)*, Honolulu, USA, pp. 546–550. doi: 10.1109/SII46433.2020.9025928.